www.cadanda.com
Computer-Aided Design AND APPLICATIONS

Customized Implant of Cervical Prostheses Exploiting a Predictive Analysis of Range of Motion

Filippo Cucinotta[1], Rosalia Mineo[2], Marcello Raffaele[3], Fabio Salmeri[4] and Felice Sfravara[5]

[1]Department of Engineering, University of Messina, ficucinotta@unime.it
[2]Mt Ortho srl, rosalia.mineo@mtortho.com
[3]Department of Engineering, University of Messina, maraffaele@unime.it
[4]Department of Engineering, University of Messina, fsalmeri@unime.it
[5]Department of Engineering, University of Messina fsfravara@unime.it

Corresponding author: Felice Sfravara, fsfravara@unime.it

Abstract. The use of arthroprosthetic devices for spinal stabilization is a widely used procedure in the field of biomechanics. There are several problems on the spinal columns that need to use devices like cages to keep distance between the vertebrae. In many cases, these devices are implanted between the vertebrae to keep a clearance between them and so avoid pain or numbness of the limbs. Thanks to new manufacturing approach, it is possible to use powerful topological optimization algorithms to get biomedical devices with high values of performance. Aim of the paper is to define a simulation to get the kinematic behavior of the human cervical structure. Thanks to the results of the simulation, the model can be used to study the effectiveness of an arthroprosthetic device positioned to stabilize the cervical segment of the spinal column and improve the rehabilitation process. The part of the vertebral column under examination is between C3 and C7. Computer Aided Design has been used starting from the 3D scan of the cervical spine obtained by magnetic resonance imaging. The great potentiality of the method is to use a kinematic simulation that models the vertebrae as rigid body and the ligaments and intervertebral discs as a system of springs. This allows to reduce the cost of simulation in term of complexity and time to reach the solution. The kinematic mechanism will be used in a second step for the assessment of the insertion of arthroprosthetic device in terms of stabilization of the upper part of the spinal column. The main objective is to have a tool that allows to immediately identify the best geometry for the patient and to optimize the shape for each specific case. The tool will be tested in future in order to verify the robustness and reliability in several other cases.

Keywords: Magnetic Resonance Imaging, Customization of Medical Devices, Kinematics, Range of Motion, Simulation.
DOI: https://doi.org/10.14733/cadaps.2023.S6.122-133

1 INTRODUCTION

The use of arthroprosthetic devices for spinal stabilization is a widely used procedure [18] in the field of biomechanics. The intervertebral body fusion devices are widely used in the treatment of diseases of the cervical [5], thoracic and lumbar [8] areas. Among the most used biocompatible materials for the realization of these devices are titanium alloys, in particular Ti-6Al-4V ELI, thanks to their high strength / weight ratio and their printability with the new Additive Manufacturing techniques [22], make it the material widely used in biomechanics. In recent decades, the development of Additive Manufacturing technologies has made possible to build complex and particularly effective structures such as rhombic dodecahedron lattices. The technologies used in this field are Electron Beam Melting (EBM), Laser Engineered Net-Shaping (LENS), and Selective Laser Melting (SLM) [21]. These technologies have allowed the development of new and increasingly powerful topological optimization algorithms[3,6,7] , but also the study of new materials for increasingly performing components also for biomedical applications [15].

Aim of the study is to model the system formed by the articulation and ligaments of the cervical tract of a human being by means of a fast and very useful kinematic model. The final kinematic model can be used for different aspects involving the problems with cervical spine. For example the development of a virtual program of exercises for personalized rehabilitation of patients, as made by Aruanno et al. [2] in the case of patients with problems to the hand. Another field of application is the evaluation of intervertebral body fusion devices in a preliminary phase in order to choose the best one for the patient. This last application will be proposed in the paper, exploiting the kinematic model developed in order to assess two different devices for treatment of diseases of cervical spine. A standard CAD model, so-called Taro, made by the University of Tokyo and obtained through magnetic resonances performed on subjects of the male population of medium height was used as the study model. The resonances were processed and a complete 3D model of the cervical spine has been obtained [14]. Thanks to this reconstruction, a kinematic model has been developed using a mix of 3D rigid bodies and 1D elastic elements. This suitably calibrated kinematic system was validated by comparison with the experimental data taken from the work of Voronov et al. [19], who conducted studies on the Range Of Motion (ROM) of the cervical tract C3-C7, belonging to cadavers, to which DTRAX® arthroposthetic devices were applied. The case studies are two different cages, made by the MtOrtho company, with the clinical purpose of solving disc disease problems on patients of two different heights i.e., 1.70 cm (case 1) and 2.00 meters (case 2). These cages were simulated by rigid bodies fixed on the vertebrae. The study of two different stature is due to the size of the different vertebrae between the northern European and southern European populations. The case of disc disease localized between C5-C6 was chosen as the implantation position. The cage (case 1) has main dimensions of about 15x15x6 mm, the cage has two different substructures, a solid structure, hereinafter referred to as "melt and a dodecahedral rhombic texture, hereinafter referred to as "net". in particular the net is a lattice structure made by Additive Manufacturing. In particular, the titanium alloy reticular bodies are used in biomechanics as casting devices, due to their biocompatibility and lightweight characteristics. The great potential of the method is that it is very fast and the implantation is very simple. The method can be used in order to calibrate rehabilitation exercise or in order to implement a virtual platform for rehabilitation as reported by Aruanno et al [1]. The future turning point is automatic learning, both for the treatment of spine surgery and the related clinical decisions to optimize post-operative results [4], but also for personalized topological optimization for the patient [20].

2 MATERIALS AND METHODS

2.1 Anatomy of the Cervical Spine

The study proposed in the paper is focused on the part of the cervical spine between C3-C7. In general, the cervical spine has 7 stacked bones called vertebrae and labeled from C1 to C7. The first one (C1) connects the neck to the skull, the last one connects the neck to the upper back (between

the shoulder). The main tasks of this part of spine are to support the movement of the head and protecting the spinal cord. There are many examples in the literature of CAD models that take advantage of Magnetic Resonance Imaging to reconstruct the cervical spine. In this paper, a polygonal reconstruction of the non-profit research institute DBCLS (Database Center for Life Science) at the University of Tokyo [13,14] has been used. The MRI images belong to an adult male with a height of 171.4 cm and with a weight of 63.3 kg. Figure 1 shows the main planes of the cervical spine, the picture 1 (d) highlights the sagittal plane and the five vertebrae with the section useful to understand all the rigid parts of the spine and the scientific nomenclature.

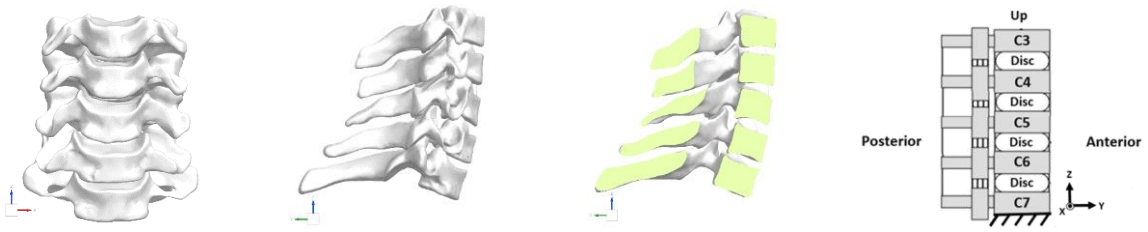

Figure 1: 3D polygonal reconstruction of the cervical spine: (a) frontal view, (b) lateral view, (c) sagittal section and (d) the scientific nomenclature.

The cervical spine under investigation in this paper has been modeled with the following anatomical structures: the cervical vertebrae from C3 to C7, the intervertebral discs subdivided into a fibrous ring (annulus) and nucleus pulposus, the ligaments. The vertebrae have been considered as rigid parts, during the movement of the head the bone is not subjected to deformations or stresses beyond the breaking point of the bone. There is other two main parts of the cervical spine: the intervertebral discs and the ligaments. The discs help to absorb eventual shocks, they have a function of cushion between vertebrae in all the activities of weight-bearing. The disc is composed by two annular parts, the outer annulus called annulus fibrosus and the inner part called nucleus pulposus, as shown in Figure 2**.**

Figure 2: Disc between C6-C7 with annulus fibrosus and nucleus pulposus.

The ligaments that participate in the kinematic of the cervical considered in the paper are: ALL (Anterior longitudinal ligament), PLL (Posterior Longitudinal Ligament), CL (Capsular ligament), CF (Flavum ligament), ISL (Interspinous ligament). There are ligaments continuous along all the cervical spine and reach the lower part of column, they are the Anterior Longitudinal Ligament (ALL), Posterior Longitudinal Ligament (PLL) and the Flavum Ligament (LF). Figure 3 shows these three ligaments in a 3D view and in a lateral view. The other two ligaments considered in the model are the Capsular Ligament (LC) and the Interspinous Ligament (ISL). These two ligaments work between two consecutives vertebrae. The Figure 4 shows an example of these two ligaments between C3-C4.

2.2 Model and Mechanical Properties

The vertebrae are modeled as a rigid part with a distributed mass. The value of mass for each cervical vertebra is reported in Table 1 as suggested by Lowrance et al. [12].

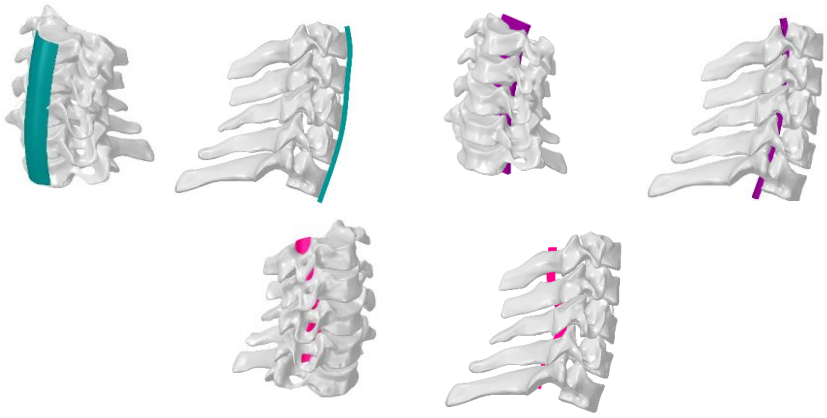

Figure 3: From top to bottom – (a) ALL, (b) PLL and (c) LF.

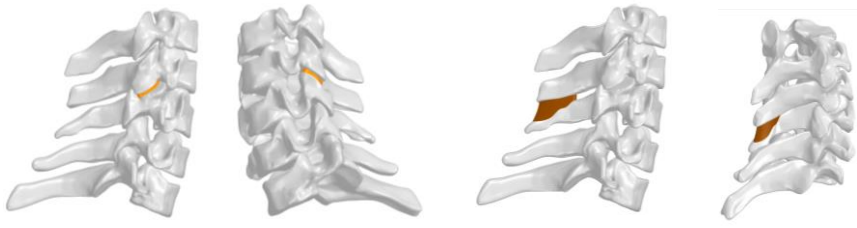

Figure 4: (a) LC between C3-C4 and (b) ISL between C3-C4.

Cervical vertebrae	*Weight [g]*
C3	4.9
C4	5.2
C5	5.4
C6	5.8
C7	6.6

Table 1: vertebrae weights.

In order to simplify and reduce the time of computation, the discs and the ligaments have been modeled with a system of springs following 1D approach, avoiding the complexity of a 3D model. The main parameter of these springs is the stiffness, the value assigned during the simulation allows to reproduce the real behavior both for the discs and the ligaments. For each part with a homogenous material has been defined a global stiffness subdivided in a number of springs working in parallel, for each single spring the value of stiffness is reported in the equation (2.1).

$$K_i = \frac{K}{n} \left[\frac{N}{mm}\right] \tag{2.1}$$

K is the overall stiffness of the homogeneous element; n is the number of springs into which the part has been divided and Ki the specific stiffness of the individual spring. The stiffness of these springs was modelled and calibrated on the basis of the available scientific literature, generally based on experimental data conducted on cadavers. The intervertebral disc was modelled by means of parallel springs differentiated in stiffness according to whether they compose the annulus or the nucleus pulposus. The intervertebral discs consist mainly of two concentric parts, the central part, formed by the nucleus pulposus, and an outer fibrous ring (annulus). The disc has been modeled

with a group of parallel springs (shown in the Figure 5); the mechanical behavior of these springs is to only react to compression forces. The direction of the springs is influenced by the surfaces of the two consecutive vertebrae.

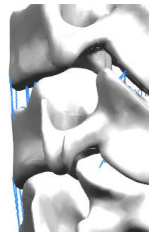

Figure 5: Parallel springs used for modeling the disk C3-C4.

The pulposus has been modeled with hyper-elastic properties (according to the Mooney-Rivlin definition of material [16]). The elastic modulus E was calculated using formula (2.2):

$$E \cong 6 \cdot (C_1 + C_2)\ [MPa] \tag{2.2}$$

The two parameters C1 and C2 (2.3), were derived from the scientific literature [16] as:

$$C_1 = 0.12 \quad e \quad C_2 = 0.09 \tag{2.3}$$

The stiffness has been calculated using the following formula (2.4), it is dependent by the section area (A) of nucleus pulposus, the value of elastic modulus calculated with (2.2) and the average height of the intervertebral disc. The last parameter has been measured thanks to the 3D model of the scan.

$$K = \frac{E \cdot A}{h} \left[\frac{N}{mm}\right] \tag{2.4}$$

The area of the nucleus pulposus was evaluated as 70% of the entire disc area, with the remaining 30% being occupied by the annulus [17]. The annulus has a fibrous structure and as reported by Ha [10] the material of this part can be modeled with a 4-layer laminated composite structure. This structure consists of matrix and fibers oriented with +/- 65° (20% volume fraction). The mechanical characteristics of matrix and fibers are indicated in Table 2 [10] calculated with the rule of mixtures.

Annulus	*Elastic module*	*Poisson's ratio*
Matrix annulus	4.2	0.45
Fiber annulus	450	0.3
Composite	4.8	0.23

Table 2: Mechanical characteristics of the annulus.

Table 3 shows the height and area values of the various intervertebral discs for each pair of vertebrae from C3 to C7. The literature suggests to divide the intervertebral disc with the 70% of area occupied by the nucleus pulposus and the remaining 30% occupied by the annulus.

Discs	*Height [mm]*	*Total area [mm²]*
C3-C4	3.5	288
C4-C5	3.5	320
C5-C6	5	327
C6-C7	4	375

Table 3: Height and area.

Table 4 shows the specific stiffness values of the nucleus pulposus and the annulus, for each disc. The table also shows the number of springs used for each disc and part of disc.

Nucleus	*Spring*	*Ki [N/mm]*
C3-C4	9	8.1
C4-C5	9	9.0
C5-C6	9	6.4
C6-C7	9	9.2
C3-C4	9	8.1

Annulus	*Spring*	*Ki [N/mm]*
C3-C4	15	7.9
C4-C5	15	8.8
C5-C6	15	6.3
C6-C7	15	9.0
C3-C4	15	7.9

Table 4: Stiffness of the nucleus (left) and annulus pulposus (right).

The same concept has been used for the ligaments. An example of the spring system used for the ligaments is reported in Figure 6. The picture shows the body-spring system formed by the couple of C3-C4 vertebrae and the interspinous ligament, ISL.

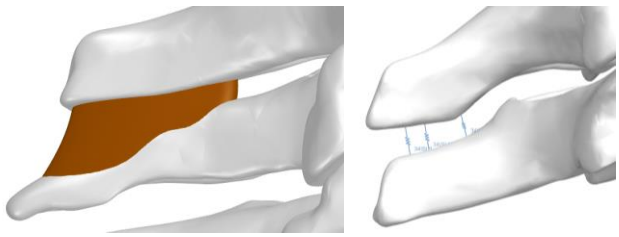

Figure 6: ISL ligament anatomically on the left, transformed into system of springs following 1D approach on the right.

The stiffness value of the springs was taken from the scientific literature [11]. The mechanical behavior of the springs is to react only to tensile forces, as for the real ligaments. Also in this case, the specific stiffness is calculated as a function of the number of elements in which the ligament is discretized. Table 5 shows the values of the stiffness for each spring used in the model.

Ligament	*Number of spring elements*	*Overall stiffness K [N/mm]*	*Specific stiffness Ki [N/mm]*
ALL	3	46.9	15.6
PLL	2	71.6	35.8
CL	3 (on each side)	69.4	23.13
LF	5	118	23.6
ISL	3	22.1	7.3

Table 5: Stiffness of the ligaments.

2.3 Constraint System, Contacts, Degrees of Freedom and Range of Motion

In order to evaluate different case studies and doing a comparison between results, the Range of Motion (ROM) must be evaluated under different load conditions. For the evaluation of ROM (Range of Motion) the experimental system used in the article [19] on cadavers was replicated in a virtual way. The degrees of freedom are the rotation around the X-axis (flexion-extension), the rotation around the Y-axis (lateral bending) and the torsion of the head around the Z-axis (axial rotation).

The load consists of a moment equal to 1.5 Nm applied on the C3 vertebra and acting individually around each axis, Figure 7 shows the definition of the Range of Motion.

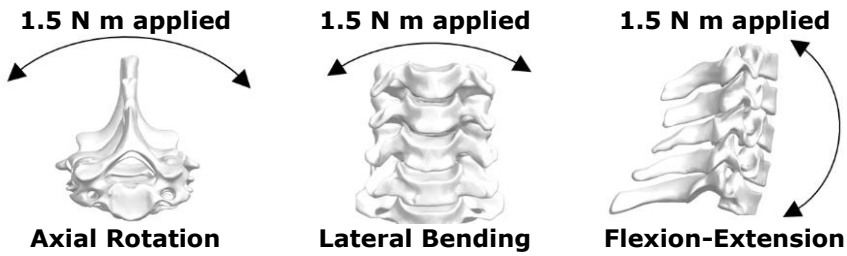

Figure 7: Definition of Range of Motion.

On the C7 vertebra there is an interlocking constraint that blocks any displacement and rotation in the three directions. No constraints are applied to the remaining vertebrae. The contact between the vertebrae was modeled with a rigid, non-penetrating and frictionless contact. The ROM allows to evaluate the flexibility of the cervical spine and thanks to results of kinematic model it is possible to get displacements, velocities and accelerations of any point considered. The data obtained are the displacement of the center of mass of each individual vertebra with relative Euler angles. The Euler angles are labeled 1, 2 and 3 and they are respectively along the x axis (flexion-extension), y (lateral bending) and z (axial rotation).

2.4 MtOrtho Device, Description and Case Studies

The MtOrtho cage in Figure 8 is positioned anteriorly between the vertebral arches of two consecutive vertebrae, allows realignment and correct spacing between two suffering vertebrae in discopathy patients. The cage has two different substructures: the solid structure (melt) and the rhombic dodecahedral texture (net).

Figure 8: The cage a with highlighted the net and melt structures.

These arthroplasty is usually made by Additive Manufacturing EBM [9] in Ti-6Al-4V ELI, the surfaces of the vertebrae in contact with the cage are scraped, this procedure is called "bleeding the bone", favoring the osseointegration of the two vertebrae with the cage, fixing them. The case studies under investigation involve two different sizes of the same device, called cage A and cage B. Cage B is obtained from an affinity scaling of cage A. Figure 9 shows the comparison between the melt structure of cage A (in green) and the one of cage B (in blue). Cage B is taller (z scale factor of 1.43), narrower (x scale factor of 0.875), and shorter (y scale factor of 0.75).

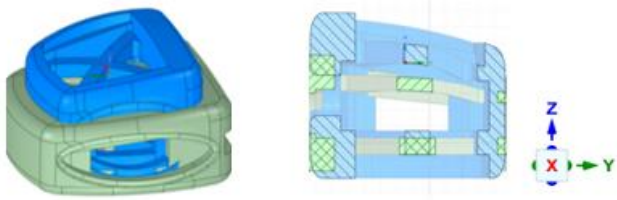

Figure 9: comparison between cage A (green) and cage B (blue).

The kinematic study was carried out with Siemens NX© Motion software. The case studies under investigation are three. The first one is the free condition (without cage between vertebrae) and the results of this case have been compared with the experimental ones proposed by Nagaoka et al. [14]. The second case is the condition with the cage A between the vertebrae C5-C6 and the third case is the condition with the cage B between the vertebrae C5-C6.

3 RESULTS AND DISCUSSION

3.1 Case Study 1: Range of Motion in Free Condition

Figure 10 shows the screenshots of animation of the motion study of the cervical spine. The pictures show the maximum rotation for each load condition applied. Thanks to these results it is possible to extract all the angles between the single vertebrae.

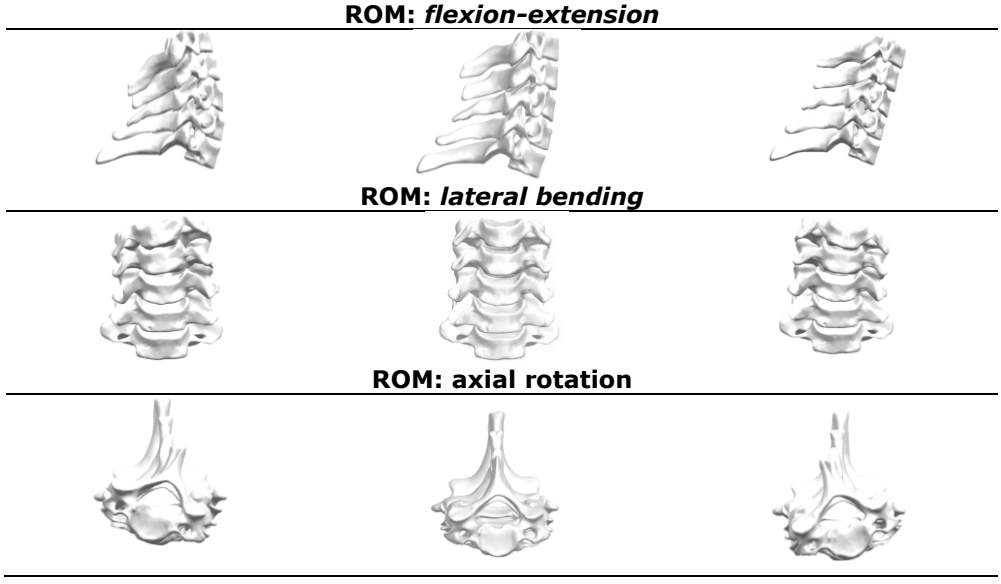

Figure 10: Extremal positions of ROM.

Table 6 shows the ROM values, considering the various segments of the cervical tract and comparing them with the experimental data [19]. The comparison with the experimental results of literature is very promising and it confirms that it is possible to simulate the kinematic of cervical spine with the use of a mix of 1D approach and 3D models.

Range of Motion [deg]		
Motion Segment	*Simulation*	*DTRAX® device Paper – Intact [12]*
C3-C4		
Flexion-extension	8.34	9.0 ± 2.5
Lateral bending	8.88	11 ± 3.0
Axial rotation	12.91	6.9 ± 2.4
C4-C5		
Flexion-extension	7.19	8.6 ± 2.0
Lateral bending	7.0	9.8 ± 1.2

Axial rotation	10.84	9.3 ± 3.2
C5-C6		
Flexion-extension	9.74	11.5 ± 3.5
Lateral bending	5.26	10 ± 2.1
Axial rotation	8.74	8.5 ± 2.1
C4-C6		
Flexion-extension	16.94	20.2 ± 5.2
Lateral bending	12.27	10.8 ± 2.6
Axial rotation	19.59	17.8 ± 5.1

Table 6: Comparison of ROM results from case study 1.

3.2 Case Study 2: Range of Motion Cage A Implanted in C5-C6

In Figure 11 it is possible to see the model of the cervical with the cage A designed by MtOrtho© and implanted in the pair of cervical vertebrae C5-C6.

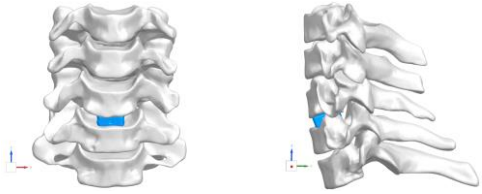

Figure 11: Case 2: cage A on cervical C5-C6.

The ROM obtained in the Table 7 are compared with those of the literature relating to the DTRAX® device.

Range of Motion [deg]		
Motion Segment	*Simulation*	*DTRAX® device Paper – Intact [12]*
C3-C4		
Flexion-extension	8.3	10 ± 2.6
Lateral bending	8.58	11.1 ± 2.5
Axial rotation	12.58	8.1 ± 2.7
C4-C5		
Flexion-extension	7.51	9.8 ± 1.8
Lateral bending	6.62	9.3 ± 1.5
Axial rotation	5.94	10.0 ± 3.3
C5-C6		
Flexion-extension	0	3.4 ± 1.8
Lateral bending	0	0.7 ± 0.5
Axial rotation	0	0.8 ± 0.5
C4-C6		
Flexion-extension	7.51	12.5 ± 3.5
Lateral bending	6.62	10.0 ± 1.6
Axial rotation	5.94	10.8 ± 3.6

Table 7: Comparison of ROM results from case study 2.

In this case study there is a value of 0 between the vertebrae C5-C6 because among these two vertebrae has been applied the cage. The main objective of the cage is to lock the relative movement of C5 and C6 and so to keep fuse the two vertebrae. This effect is evident in the DTRAX® case, where there is a great reduction of mobility with respect to the free case. The simulation also models this effect. The DTRAX® case has been conducted on "*ex vivo*" considering all the ligaments of the spine cervical with the correct direction of force reaction. The model proposed in this paper lacks of some ligaments and the direction of the springs is not equal to the one considered in DTRAX® case, this discrepancy could lead to the differences reported in Table 7.

3.3 Case Study 3: Range of Motion Cage B Implanted in C5-C6

In case study 3, the cervical spine is considered in relation to a patient who is 2.00 meters tall and has an intervertebral cage B at C5-C6. The ROM obtained in the Table 8 are compared with the ones of the literature relating to the DTRAX® device.

Range of Motion [deg]		
Motion Segment	*Simulation*	*DTRAX® device Paper – Intact [12]*
C3-C4		
Flexion-extension	6.6	10 ± 2.6
Lateral bending	7.43	11.1 ± 2.5
Axial rotation	9.46	8.1 ± 2.7
C4-C5		
Flexion-extension	6.77	9.8 ± 1.8
Lateral bending	7.698	9.3 ± 1.5
Axial rotation	12.88	10.0 ± 3.3
C5-C6		
Flexion-extension	0	3.4 ± 1.8
Lateral bending	0	0.7 ± 0.5
Axial rotation	0	0.8 ± 0.5
C4-C6		
Flexion-extension	6.77	12.5 ± 3.5
Lateral bending	7.698	10.0 ± 1.6
Axial rotation	12.90	10.8 ± 3.6

Table 8: Comparison of ROM results from case study 3.

Also, in this case study there is a value of 0 between the vertebrae C5-C6 because among these two vertebrae has been applied the cage. For the same reasons of case study 2 there is a discrepancy between the simulation and the test case of DTRAX®.

4 CONCLUSION

The kinematic study of the cervical spine examined simulates with good approximation the real behavior of the spinal column. The findings of this method are promising and a good correlation was found with experimental results proposed in literature. Compared to a FEM system, the kinematic model is considerably more efficient in terms of computational cost, calculation time and complexity in the setup phase. Thanks to this kinematic model has been possible to evaluate the efficiency of different cage devices developed by MtOrtho applied to two patients with different height and cervical discopathy. The cages provide a good stability of the section on which they act without excessively reducing the Range of Motion (ROM) of the column in the free vertebrae sections. Further

investigations will be necessary to improve the kinematic model considering muscles and ligaments not considered in this phase.

Filippo Cucinotta, http://orcid.org/0000-0002-0304-4004
Marcello Raffaele, http://orcid.org/0000-0003-0638-1919
Fabio Salmeri, http://orcid.org/0000-0002-8803-4795
Felice Sfravara, http://orcid.org/0000-0003-3922-8494

REFERENCES

[1] Aruanno, B.; Caruso, G.; Rossini, M.; Molteni, F.; Espinoza, M.C.E.; Covarrubias, M.: Virtual and Augmented Reality Platform for Cognitive Tele-Rehabilitation Based System, in: 2020: pp. 130–137. https://doi.org/10.1007/978-3-030-58796-3_17.

[2] Aruanno, B.; Covarrubias, M.: HANDY: Novel Hand Exoskeleton for Personalized Rehabilitation, Comput. Aided. Des. Appl. 19 (2021) 405–425. https://doi.org/10.14733/cadaps.2022.405-425.

[3] Barberi, E.; Cucinotta, F.; Raffaele, M.; Salmeri, F.: A Hollowing Topology Optimization Method for Additive and Traditional Manufacturing Technologies, in: Lect. Notes Mech. Eng., 2022. https://doi.org/10.1007/978-3-030-91234-5_43.

[4] Chang, M.; Canseco, J.A.; Nicholson, K.J.; Patel, N.; Vaccaro, A.R.: The Role of Machine Learning in Spine Surgery: The Future Is Now, Front. Surg. 7 (2020). https://doi.org/10.3389/fsurg.2020.00054.

[5] Cucinotta, F.; Mineo, R.; Raffaele, M.; Salmeri, F.: Assessment of the run-out of an intervertebral cervical cage fabricated by additive manufacturing using electron beam melting, in: Proc. ASME Des. Eng. Tech. Conf., 2021. https://doi.org/10.1115/DETC2021-70241.

[6] Cucinotta, F.; Raffaele, M.; Salmeri, F.: A stress-based topology optimization method by a Voronoi tessellation Additive Manufacturing oriented, Int. J. Adv. Manuf. Technol. 103 (2019) 1965–1975. https://doi.org/10.1007/s00170-019-03676-4.

[7] Cucinotta, F.; Raffaele, M.; Salmeri, F.: A Topology Optimization Method for Stochastic Lattice Structures, in: 2021: pp. 235–240. https://doi.org/10.1007/978-3-030-70566-4_38.

[8] Epasto, G.; Distefano, F.; Mineo, R.; Guglielmino, E.: Subject-specific finite element analysis of a lumbar cage produced by electron beam melting, Med. Biol. Eng. Comput. 57 (2019) 2771–2781. https://doi.org/10.1007/s11517-019-02078-8.

[9] Galati, M.; Iuliano, L.: A literature review of powder-based electron beam melting focusing on numerical simulations, Addit. Manuf. 19 (2018) 1–20. https://doi.org/10.1016/j.addma.2017.11.001.

[10] Ha, S.K.: Finite element modeling of multi-level cervical spinal segments (C3-C6) and biomechanical analysis of an elastomer-type prosthetic disc, Med. Eng. Phys. 28 (2006) 534–541. https://doi.org/10.1016/j.medengphy.2005.09.006.

[11] Ivancic, P.C.; Coe, M.P.; Ndu, A.B.; Tominaga, Y.; Carlson, E.J.; Rubin, W.; Dipl-Ing, F.H.; Panjabi, M.M.: Dynamic mechanical properties of intact human cervical spine ligaments, Spine J. 7 (2007) 659–665. https://doi.org/10.1016/j.spinee.2006.10.014.

[12] Lowrance, E.W.; Latimer, H.B.: Weights and variability of components of the human vertebral column, Anat. Rec. 159 (1967) 83–88. https://doi.org/10.1002/ar.1091590112.

[13] Mitsuhashi, N.; Fujieda, K.; Tamura, T.; Kawamoto, S.; Takagi, T.; Okubo, K.: BodyParts3D: 3D structure database for anatomical concepts, Nucleic Acids Res. 37 (2009) 782–785. https://doi.org/10.1093/nar/gkn613.

[14] Nagaoka, T.; Watanabe, S.; Sakurai, K.; Kunieda, E.; Watanabe, S.; Taki, M.; Yamanaka, Y.: Development of realistic high-resolution whole-body voxel models of Japanese adult males and females of average height and weight, and application of models to radio-frequency electromagnetic-field dosimetry, Phys. Med. Biol. 49 (2004) 1–15. https://doi.org/10.1088/0031-9155/49/1/001.

[15] Puleio, F.; Rizzo, G.; Nicita, F.; Lo Giudice, F.; Tamà, C.; Marenzi, G.; Centofanti, A.; Raffaele, M.; Santonocito, D.; Risitano, G.: Chemical and mechanical roughening treatments of a supra-nano composite resin surface: SEM and topographic analysis, Appl. Sci. 10 (2020) 1–9. https://doi.org/10.3390/app10134457.

[16] Schmidt, H.; Heuer, F.; Simon, U.; Kettler, A.; Rohlmann, A.; Claes, L.; Wilke, H.J.: Application of a new calibration method for a three-dimensional finite element model of a human lumbar annulus fibrosus, Clin. Biomech. 21 (2006) 337–344. https://doi.org/10.1016/j.clinbiomech.2005.12.001.

[17] Toosizadeh, N.; Haghpanahi, M.: Generating a finite element model of the cervical spine: Estimating muscle forces and internal loads, Sci. Iran. 18 (2011) 1237–1245. https://doi.org/10.1016/j.scient.2011.10.002.

[18] Türeyen, K.; Maciejczak, A.: Disc height loss after anterior cervical microdiscectomy with titanium intervertebral cage fusion, Acta Neurochir. (Wien). 145 (2003) 565–570. https://doi.org/10.1007/s00701-003-0050-1.

[19] Voronov, L.I.; Siemionow, K.B.; Havey, R.M.; Carandang, G.; Patwardhan, A.G.: Biomechanical evaluation of DTRAX® posterior cervical cage stabilization with and without lateral mass fixation, Med. Devices Evid. Res. 9 (2016) 285–290. https://doi.org/10.2147/MDER.S111031.

[20] Wong, A.Y.L.; Harada, G.; Lee, R.; Gandhi, S.D.: A. Dziedzic, A. Espinoza-Orias, M. Parnianpour, P.K. Louie, B. Basques, H.S. An, D. Samartzis, Preoperative paraspinal neck muscle characteristics predict early onset adjacent segment degeneration in anterior cervical fusion patients: A machine-learning modeling analysis, J. Orthop. Res. 39 (2021) 1732–1744. https://doi.org/10.1002/jor.24829.

[21] Xiao, L.; Song, W.; Wang, C.; Liu, H.; Tang, H.; Wang, J.: Mechanical behavior of open-cell rhombic dodecahedron Ti-6Al-4V lattice structure, Mater. Sci. Eng. A. 640 (2015) 375–384. https://doi.org/10.1016/j.ijimpeng.2016.10.006.

[22] Xiao, L.; Song, W.; Wang, C.; Tang, H.; Fan, Q.; Liu, N.; Wang, J.; Mechanical properties of open-cell rhombic dodecahedron titanium alloy lattice structure manufactured using electron beam melting under dynamic loading, Int. J. Impact Eng. 100 (2017) 75–89. https://doi.org/10.1016/j.msea.2015.06.018.